

Observation of Unidirectional s-p Orbital Topological Edge States in Driven Photonic Lattices

Gayathry Rajeevan¹ and Sebabrata Mukherjee^{1,*}

¹*Department of Physics, Indian Institute of Science, Bangalore 560012, India*

(Dated: January 15, 2026)

Time-periodic modulation of a static system is a powerful method for realizing robust unidirectional topological states. So far, all such realizations have been based on interactions among *s* orbitals, without incorporating inter-orbital couplings. Here, we demonstrate higher-orbital Floquet topological insulators by introducing periodically modulated couplings between the optical *s* and *p* orbitals in a square lattice. The staggered phase of the *s-p* couplings gives rise to a synthetic uniform π magnetic flux per plaquette of the lattice, and periodic driving of the couplings opens a topological bandgap, characterized by the Floquet winding number. We image topological edge modes of *s-p* orbitals traveling unidirectionally around a corner. Here, the topological phases are realized by a combined effect of the periodic driving and synthetic magnetic flux. Consequently, when the synthetic flux is turned off, the system becomes trivial over a range of driving parameters. Our results open a promising pathway for exploring topological phenomena by introducing the orbital degree of freedom.

* mukherjee@iisc.ac.in

Introduction

Topological states were originally observed in two-dimensional electron gases under a strong transverse magnetic field, which breaks the time-reversal symmetry [1, 2]. Since then, various intriguing topological phases have been realized in a wide range of experimental settings [3–10], including ultra-cold atoms and photonics systems. Specifically, topological photonics [11–14] has recently emerged as an important subfield of modern optics, uncovering novel physics and holding a great promise for robust device applications [15, 16].

Periodically driving a system’s Hamiltonian – known as Floquet engineering [17–19] – is a powerful and convenient tool for creating topologically non-trivial materials. For example, photonic Chern insulators [4] have been realized by helically modulating the waveguide paths of a honeycomb lattice, and anomalous Floquet topological insulators, which has no static analogue, were observed in slowly-driven lattices [20–23]. Such Floquet topological states have been demonstrated in engineered lattice systems where each site usually supports a single state, i.e., the s -orbital. Although experimentally challenging, the incorporation of higher-orbital interactions into these driven systems can provide an additional degree of controllability in exploring novel topological phases [24, 25]. The orbital physics plays an important role in understanding a variety of condensed matter systems, ranging from transition-metal oxides [26] to orbital superfluids [27]. In photonics, higher orbitals have been exploited in band engineering [28, 29] and to create synthetic magnetic flux [30, 31]; see also [32, 33]. Additionally, zero-dimensional topological edge states have been studied in static systems [34–36] with inter-orbital couplings. Such couplings have also found promising applications in the design of compact photonic devices [37–39].

In this work, we experimentally demonstrate two-dimensional higher-orbital Floquet topological insulators making use of the engineered couplings between the optical s and p_y (hereafter referred to as p) orbitals of neighboring sites. The photonic lattices are fabricated using femtosecond laser-writing [40, 41], which allows us to fine-tune the waveguide refractive index profiles and precisely modulate the waveguide paths to enable periodically modulated s - p orbital couplings. We implement a four-step driving protocol where the s - p couplings are switched on and off in a cyclic manner. Unlike the previous works [20–22] on anomalous Floquet topological insulators, one vertical coupling in each plaquette of the lattice is made negative by utilizing the odd parity of p orbitals, resulting

in a uniform synthetic π magnetic flux. The periodic driving, along with the synthetic flux, realizes topological phases characterized by the Floquet winding numbers. Specifically, as the driving parameter is tuned, the system undergoes transitions from a Chern insulator to anomalous Floquet topological insulator and subsequently back to a Chern insulator. In experiments, we image the topological edge modes of s - p orbitals traveling around a corner of the lattice. To highlight the importance of the synthetic magnetic flux, we also demonstrate the existence of such unidirectional edge modes using certain parameters for which the system becomes trivial when the s - p orbital couplings are replaced by s - s couplings with vanishing flux.

Results

Model – We consider a photonic square lattice consisting of two sites (A and B) per unit cell, as illustrated in Fig. 1(a). The A site supports only the fundamental mode (s orbital) with on-site energy β_s^A , while the B site supports both the s and p orbitals with on-site energies β_s^B and β_p^B , respectively. The s orbital of A sites and the p orbital of B sites are phase-matched (i.e., $\beta_s^A = \beta_p^B$), whereas the on-site energy of the s orbital of the B site is largely detuned. In this situation, an initial state localized at the A site can tunnel only to the p orbital of a neighboring B site, while the s orbital of the B site remains effectively decoupled. Hence, we shall consider the tunneling of light among these s and p orbitals of A and B sites, respectively.

The s - p orbital couplings in the lattice are modulated periodically along the propagation distance z in a clockwise manner. The total driving period z_0 is equally divided into four steps, and during the m -th step, i.e., $(m-1)z_0/4 \leq z \leq mz_0/4$, only $J_m^{sp}(z)$ couplings are switched on; $m = 1, 2, 3$, and 4. Note that each lattice site is coupled only to one of its nearest neighbor at a given z , and the optical power transferred from one waveguide to its nearest neighbor is determined by the parameter $\Lambda_m = |\int J_m^{sp}(z) dz|$, where the integral is carried over the m -th quarter of the driving period. In the scalar-paraxial approximation, the propagation of optical fields through the photonic lattice can be described by the following discrete Schrödinger-like equation [42]

$$i \frac{\partial}{\partial z} \psi_j(z) = -\beta_j \psi_j - \sum_{\langle j' \rangle} J_m^{sp}(z) \psi_{j'} , \quad (1)$$

where ψ_j is the envelope of the optical field at the j -th waveguide. Here, the propagation

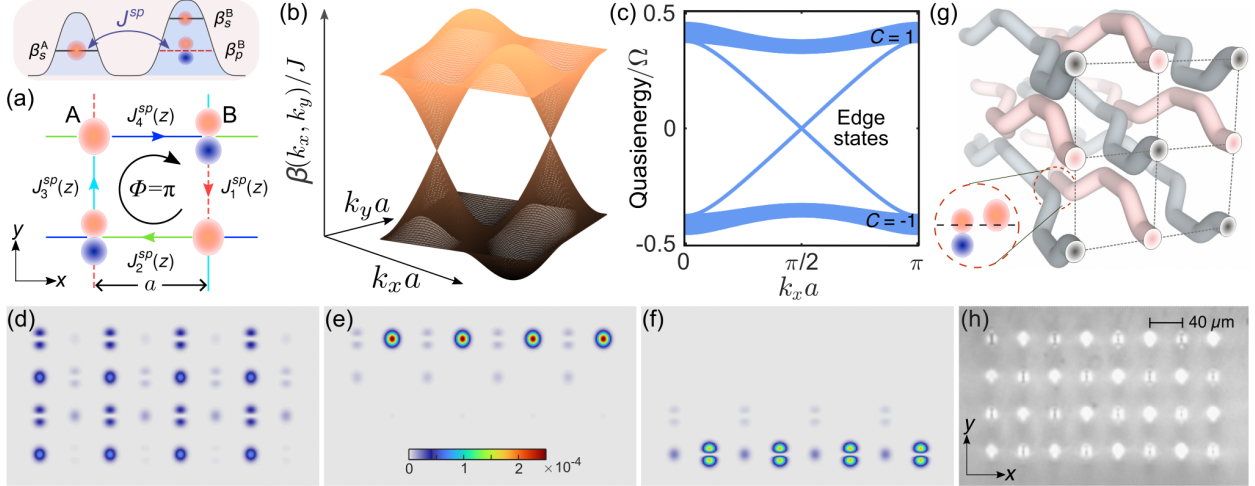


Figure 1. Photonic Floquet topological insulator of s - p orbitals. (a) Schematic of a square lattice of s - p orbitals with two sites (A and B) per unit cell and nearest-neighbor couplings J_{1-4}^{sp} . Note that J_1^{sp} is negative, realizing a uniform synthetic π magnetic flux per plaquette. The inset on the top shows the refractive index profile and the resonance condition, $\beta_s^A = \beta_p^B$. (b) Photonic bands of propagation constant $\beta(k_x, k_y)$ (analogous ‘energy’) for homogeneous coupling strengths $|J_{1-4}^{sp}| = J$, exhibiting two Dirac cones at $(k_x a, k_y a) = (\pm\pi/2, 0)$ with linear dispersion. The system in (a) is made topological by periodically switching on and off the couplings (one at a time) in a clockwise manner along the propagation distance, z . (c) Quasienergy spectrum for a strip geometry along the y direction of the Floquet square lattice with experimentally realized parameter $\Lambda_{1-4} = 0.76 \pi/2$. (d-f) Intensity distributions of bulk and edge modes (on the top and bottom edges) of s - p orbitals, respectively. (g) Simplified sketch showing the photonic realization of the Floquet topological insulator of s - p orbitals. The coupling between any two sites is switched on and off by synchronously bending the waveguide paths along z . Non-zero horizontal couplings are realized by changing the waveguide positions as indicated in the inset. (h) White-light transmission micrograph (cross-section) of a femtosecond laser fabricated s - p orbital square lattice.

distance plays the role of time ($z \leftrightarrow t$), and the propagation constant β of a photonic orbital is the analogous on-site energy. Since the lobes of the p orbital are π out of phase, the vertical coupling J_1^{sp} is negative, and the other three couplings J_{2-3}^{sp} are positive, producing a uniform synthetic magnetic π flux per plaquette of the square lattice. In other words, when the optical field encircles a closed loop around a plaquette, it acquires a π phase – analogous to the Aharonov-Bohm phase [43]. In the absence of the periodic modulation, the Fourier-

space static Hamiltonian $\hat{H}(k_x, k_y)$ of the square lattice with π flux supports two inequivalent Dirac points [44] at $(k_x a, k_y a) = (\pm\pi/2, 0)$, where $\mathbf{k} = (k_x, k_y)$ is the quasimomentum and, a is the lattice constant; see Fig. 1(b). In this situation, the application of z -periodic modulation to the couplings effectively breaks *time* reversal symmetry, thereby opening a topological gap around the quasienergy $\varepsilon = 0$, as described below.

For our z -periodic photonic structure with $\hat{H}(z + z_0) = \hat{H}(z)$, the evolution operator is defined as [17]

$$\hat{U}(z) = \mathcal{T} \exp \left[-i \int_0^z dz' \hat{H}(z') \right],$$

where \mathcal{T} is z -ordering. Considering a strip-geometry aligned along the y direction, and periodic along the x direction, we calculate the quasienergy spectrum by diagonalizing the evolution operator $\hat{U}(z_0)$ over one complete period. In Fig. 1(c), the spectrum is shown for $\Lambda_{1-4} \equiv \Lambda = 0.76 \pi/2$, where topological edge modes appear in the quasienergy gap around $\varepsilon = 0$. In Figs. 1(d-f), we show the intensity distributions of bulk and edge modes (on the top and bottom edges) considering the experimentally realized system size and with periodic boundary condition in the x direction. Notice the mixing of s - p orbitals in forming the bulk and edge states. Additionally, for our driving parameters, the s (p) orbitals exhibit a higher weightage in the top (bottom) edge, indicating the possibility of exciting these modes using a single-site initial state.

The topology of our system is captured by the integer-valued Floquet winding number, which takes into account the complete z evolution of the Floquet operator $\hat{U}(z)$ [21]. Specifically, the winding number for a quasienergy gap is equal to the number of topological edge modes in that gap. In the case of Fig. 1(c), the winding number for the bandgap around zero quasienergy $W_{\varepsilon=0}$ is unity, as there exists one topological edge mode in this gap. The other bandgap around quasienergy $\varepsilon = \pm\Omega/2$ is trivial, as no topological edge states exist in this gap, meaning $W_{\varepsilon=\pm\Omega/2} = 0$. The winding numbers can be related to the standard topological invariant, i.e., the Chern number. Indeed, a Floquet quasienergy band can also be characterized by the Chern numbers \mathcal{C} , which is equal to the difference of the winding numbers below and above that band. Evidently, the Chern number of the upper band of our driven s - p lattice is unity. It should be noted that, away from the high-frequency driving limit, as in our case, driven systems can support anomalous Floquet topological edge states, when the Chern numbers are zero for all of the

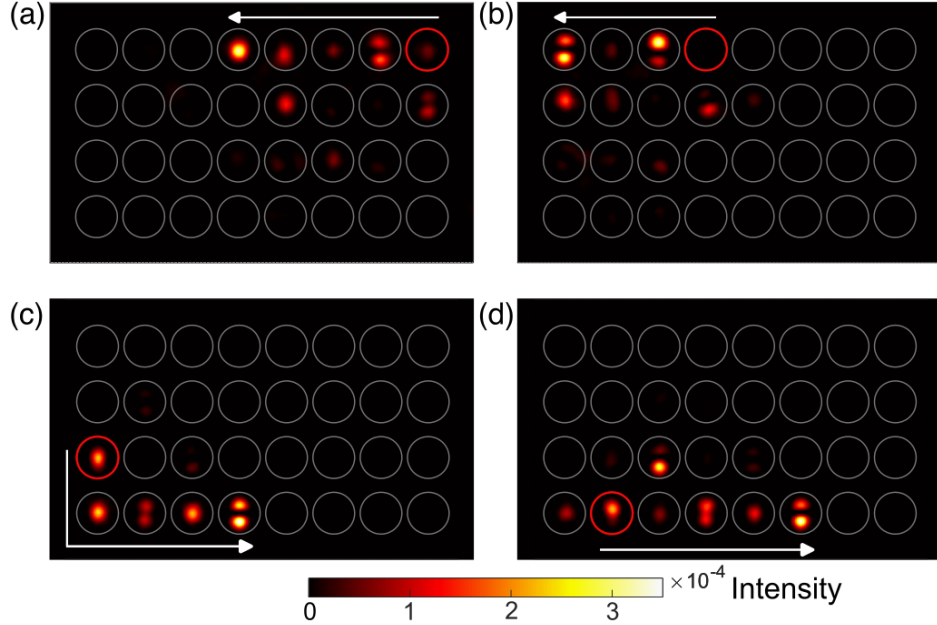


Figure 2. Probing unidirectional s - p orbital topological edge states. Experimentally measured output intensity distributions at $z = 2z_0$. Here, $\Lambda = (0.76 \pm 0.02)\pi/2$. The red circle marks the input coupling position. In (a) and (b), the light is coupled to the s mode of A sites at the input, whereas in (c) and (d), it is mostly ($\sim 81\%$) coupled to the p mode of B sites. The topological edge modes propagate unidirectionally and are not scattered by corners. Each measured intensity pattern is normalized to 1.

Floquet bands [21, 45].

Experiments – In experiments, the coupling between any two sites is switched on and off by synchronously bending the waveguide paths as depicted in Fig. 1(g). The coupling strength decays exponentially as a function of the inter-waveguide spacing. Hence, the inter-waveguide spacing is first reduced, then kept fixed for a certain propagation distance L and finally increased in a reverse manner to obtain a step-like variation of the couplings along z . The Λ_m -values are controlled by varying the straight sections L of the coupling. Since the overlap integral of the orbitals determines the inter-orbital s - p coupling, the coupling depends heavily on the orientation of the waveguides and the supported modes [46]. To achieve non-zero horizontal couplings ($J_{2,4}^{sp}$) in the lattice, we keep the waveguides at a 45 deg angle in the coupling region with the same orientation of the orbitals as indicated in the inset of Fig. 1(g); see also Supplementary Fig. S1.

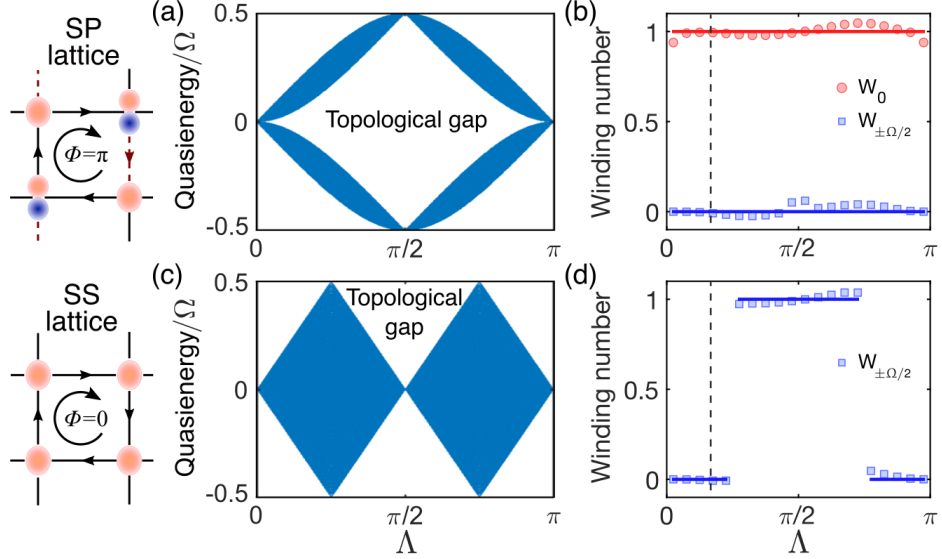


Figure 3. Topological invariants. (a) Bulk quasienergy spectrum of the *s-p* lattice as a function of Λ showing the bandgap closing and opening, which indicates topological phase transitions. (b) Winding numbers W_ε for the gaps centered around quasienergy $\varepsilon=0$ and $\pm\Omega/2$ for the *s-p* lattice. The solid lines are guides to the eye. (c, d) Similar calculations for a lattice with *s-s* couplings with zero flux. The quasienergy gap $\varepsilon = \pm\Omega/2$ is topological for $\pi/4 < \Lambda < 3\pi/4$. The dashed vertical lines in (b, d) indicate Λ values used in Figs. 4 (a, b).

To experimentally probe the topological edge states of *s-p* orbitals, modulated photonic square lattices consisting of 32 waveguides and two driving periods were created using fs laser-writing in a 120-mm-long BK7 glass substrate, see the white-light facet image (cross-section) in Fig. 1(h). The waveguides were created using a fixed laser power, and the phase-matching of orbitals was achieved by controlling the speed at which the glass material is translated through the focus of the laser beam during the fabrication; see Supplementary Sections A and B. All transport experiments were performed using horizontally-polarized low-power light at 980 nm wavelength. Fig. 2 shows the topological edge states of *s-p* orbitals propagating in the anti-clockwise direction. The red circle indicates the site where a Gaussian input state is launched at the input. In these experiments, single-site excitation at the A site on the top edge efficiently overlaps (72%) with the topological edge states, making the output state mostly localized along the edge sites in Figs. 2(a-b). In the case of Figs. 2(c-d), the input state is primarily launched to the *p* orbital of the B site by vertically shifting the position of the input beam. Notice that the small amount ($19 \pm 4\%$) of optical

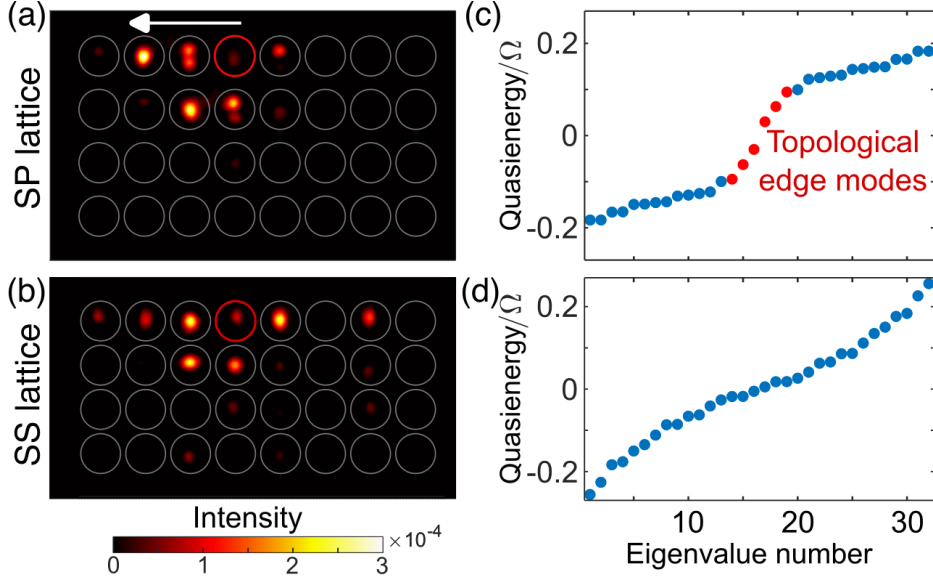


Figure 4. Importance of synthetic π flux. (a) Experimental signature of Floquet topological edge modes in a s - p orbital lattice with $\Lambda = (0.3 \pm 0.04)\pi/2$. (b) Same as (a) but in a lattice consisting of s -orbitals only with $\Lambda = (0.3 \pm 0.03)\pi/2$. In this case, the lattice is trivial as indicated by the near-symmetric (i.e., not unidirectional) spreading of the output intensity pattern along the edge. Each measured intensity pattern is normalized to 1. (c, d) Quasienergy spectrum associated with (a, b), respectively, further highlighting the topological characteristics of the lattices

power, initially coupled to the s orbital of the B site, remains localized and does not take part in the dynamics; see Supplementary Section B. The experimental observation of back-scatter-immune propagation of topological edge modes agrees well with numerical results (Eq. (1)).

Importance of π flux – Fig. 3(a) depicts the bulk quasienergy spectrum of the s - p lattice, obtained from the k -space evolution operator over one complete period $\hat{U}(\mathbf{k}, z_0)$, as a function of Λ . Here, the bandgap closing and opening indicate topological phase transitions. For each Λ value, the existence of chiral topological edge modes can be verified from the spectrum of a strip geometry. Additionally, we numerically calculated [21] winding numbers considering the full z -evolution of $\hat{U}(\mathbf{k}, z)$ for a complete period; see Figure 3(b). The quasienergy gap around $\varepsilon = 0$ hosts a topological edge mode propagating in the counter-clockwise direction for $0 < \Lambda < \pi$. Evidently, the winding number is one (zero) for the gap around $\varepsilon = 0$ ($\pm \Omega/2$).

Interestingly, the system becomes an anomalous Floquet topological insulator near $\Lambda = \pi/2$, when the quasienergy gap around $\varepsilon = \pm\Omega/2$ closes. In this case, the system is topological; however, the Chern number of the bulk band is zero.

To highlight the importance of the synthetic magnetic flux in realizing the above topological phases in the *s-p* lattice, we now consider an *s-s* lattice with vanishing flux. In other words, consider a square lattice with the same driving protocol, where all couplings take positive values. In this case, the bandgap closing/opening and the topological phases are different, as shown in Figs. 3(c, d). As Λ is tuned, the overall bandwidth of the single bulk band changes linearly, realizing only the anomalous Floquet topological phase for $\pi/4 < \Lambda < 3\pi/4$. The winding number $W_{\varepsilon=\pm\Omega/2}$ is unity for this range of Λ . Evidently, the presence of π flux in the *s-p* lattice not only alters the topological characteristics but also broadens the range of Λ for which the system is topological. Although we focus on the *s-s* lattice in Figs. 3(c, d) for experimental convenience, a similar driven square lattice with zero flux per plaquette can be realized using *s-p* orbitals. This can be achieved by rotating the *p* orbitals by 45 deg with respect to the vertical axis.

To experimentally demonstrate this, we fabricated *s-p* and *s-s* lattices with a Λ value near $0.3\pi/2$, see the vertical dashed line in Figs. 3(b, d). As shown in Fig. 4(a), the *s-p* lattice exhibits unidirectional edge transport, along with some bulk penetration, as the single-site initial state has a relatively lower overlap (33%) with the topological edge modes compared to Figs. 2(a, b). On the other hand, for the *s-s* lattice, the initial state does not propagate unidirectionally along the edge. Instead, the optical field spreads almost symmetrically along the edge and diffracts into the bulk, indicating the absence of topological edge states, see Fig. 4(b). The associated quasienergy spectra for the experimentally realized parameters are presented in Figs. 4(c, d), clearly showing the topological characteristics of the two lattices. If propagated longer in larger systems, all the light in Fig. 4(b) would travel into the bulk of the system, whereas topological edge transport along with some bulk spreading would appear in the case of Fig. 4(a). The observed intensity patterns in Fig. 4 and their agreement with numerical results (see Supplementary Fig. S5) clearly indicate the presence of topological edge states in the *s-p* lattice with π synthetic flux.

Discussion

The demonstration of unidirectional *s-p* orbital Floquet topological edge modes opens a

new direction in the field of topological photonics. Specifically, accessing other higher-order orbitals and enabling novel inter-orbital coupling mechanisms [47] can be of great importance. Higher orbitals can naturally exhibit orbital degeneracy, strongly anisotropic couplings, and intrinsic orbital angular momentum. As a result, orbital degrees of freedom can unlock a wide range of lattice phenomena inaccessible to *s*-orbital-only models. Additionally, the nonlinear interactions [39, 48–51] are largely influenced by the spatial extent of the photonic orbitals, making such systems well-suited for exploring topological phenomena in the presence of engineered nonlinearity.

Acknowledgments.— We thank Bhoomija Chaurasia, Diptiman Sen, and Abhinav Sinha for helpful discussions. S.M. gratefully acknowledges support from the Ministry of Education, Government of India, through the STARS program (MoE-STARS/STARS-2/2023-0716); the Indian Institute of Science (IISc) through a start-up grant; and the Infosys Foundation, Bangalore. G.R. thanks IISc for a Ph.D. scholarship.

Data availability.— The data supporting the findings of this study are included within the article and its supplementary information. Raw datasets are available from the corresponding author upon reasonable request.

Competing financial interests.— The authors declare no competing financial interests.

- [1] K. v. Klitzing, G. Dorda, and M. Pepper, New Method for High-Accuracy Determination of the Fine-Structure Constant Based on Quantized Hall Resistance, *Phys. Rev. Lett.* **45**, 494 (1980).
- [2] D. J. Thouless, M. Kohmoto, M. P. Nightingale, and M. den Nijs, Quantized Hall Conductance in a Two-Dimensional Periodic Potential, *Phys. Rev. Lett.* **49**, 405 (1982).
- [3] Z. Wang, Y. Chong, J. D. Joannopoulos, and M. Soljačić, Observation of unidirectional backscattering-immune topological electromagnetic states, *Nature* **461**, 772 (2009).
- [4] M. C. Rechtsman, J. M. Zeuner, Y. Plotnik, Y. Lumer, D. Podolsky, F. Dreisow, S. Nolte, M. Segev, and A. Szameit, Photonic Floquet topological insulators, *Nature* **496**, 196 (2013).
- [5] M. Hafezi, S. Mittal, J. Fan, A. Migdall, and J. Taylor, Imaging topological edge states in

silicon photonics, *Nat. Photonics* **7**, 1001 (2013).

[6] G. Jotzu, M. Messer, R. Desbuquois, M. Lebrat, T. Uehlinger, D. Greif, and T. Esslinger, Experimental realization of the topological Haldane model with ultracold fermions, *Nature* **515**, 237 (2014).

[7] R. Süssstrunk and S. D. Huber, Observation of phononic helical edge states in a mechanical topological insulator, *Science* **349**, 47 (2015).

[8] T. Karzig, C.-E. Bardyn, N. H. Lindner, and G. Refael, Topological Polaritons, *Phys. Rev. X* **5**, 031001 (2015).

[9] J. Ningyuan, C. Owens, A. Sommer, D. Schuster, and J. Simon, Time- and Site-Resolved Dynamics in a Topological Circuit, *Phys. Rev. X* **5**, 021031 (2015).

[10] K. Wintersperger, C. Braun, F. N. Ünal, A. Eckardt, M. Di Liberto, N. Goldman, I. Bloch, and M. Aidelsburger, Realization of an anomalous Floquet topological phases with ultracold atoms, *Nat. Phys.* **16**, 1058 (2020).

[11] S. Raghu and F. D. M. Haldane, Analogs of quantum-Hall-effect edge states in photonic crystals, *Phys. Rev. A* **78**, 033834 (2008).

[12] L. Lu, J. D. Joannopoulos, and M. Soljačić, Topological photonics, *Nat. Photonics* **8**, 821 (2014).

[13] T. Ozawa, H. M. Price, A. Amo, N. Goldman, M. Hafezi, L. Lu, M. C. Rechtsman, D. Schuster, J. Simon, O. Zilberberg, and I. Carusotto, Topological photonics, *Rev. Mod. Phys.* **91**, 015006 (2019).

[14] D. Smirnova, D. Leykam, Y. Chong, and Y. Kivshar, Nonlinear topological photonics, *Appl. Phys. Rev.* **7**, 021306 (2020).

[15] M. Hafezi, E. A. Demler, M. D. Lukin, and J. M. Taylor, Robust optical delay lines with topological protection, *Nat. Phys.* **7**, 907 (2011).

[16] M. A. Bandres, S. Wittek, G. Harari, M. Parto, J. Ren, M. Segev, D. N. Christodoulides, and M. Khajavikhan, Topological insulator laser: Experiments, *Science* **359**, 4005 (2018).

[17] N. Goldman and J. Dalibard, Periodically Driven Quantum Systems: Effective Hamiltonians and Engineered Gauge Fields, *Phys. Rev. X* **4**, 031027 (2014).

[18] A. Eckardt, *Colloquium*: Atomic quantum gases in periodically driven optical lattices, *Rev. Mod. Phys.* **89**, 011004 (2017).

[19] I. L. Garanovich, S. Longhi, A. A. Sukhorukov, and Y. S. Kivshar, Light propagation and

localization in modulated photonic lattices and waveguides, *Phys. Rep.* **518**, 1 (2012).

[20] S. Mukherjee, A. Spracklen, M. Valiente, E. Andersson, P. Öhberg, N. Goldman, and R. R. Thomson, Experimental observation of anomalous topological edge modes in a slowly driven photonic lattice, *Nat. Commun.* **8**, 13918 (2017).

[21] M. S. Rudner, N. H. Lindner, E. Berg, and M. Levin, Anomalous Edge States and the Bulk-Edge Correspondence for Periodically Driven Two-Dimensional Systems, *Phys. Rev. X* **3**, 031005 (2013).

[22] L. J. Maczewsky, J. M. Zeuner, S. Nolte, and A. Szameit, Observation of photonic anomalous Floquet topological insulators, *Nat. Commun.* **8**, 13756 (2017).

[23] S. Mukherjee and M. C. Rechtsman, Period-doubled Floquet solitons, *Optica* **10**, 1310 (2023).

[24] X. Li and W. V. Liu, Physics of higher orbital bands in optical lattices: a review, *Rep. Prog. Phys.* **79**, 116401 (2016).

[25] T. Müller, S. Fölling, A. Widera, and I. Bloch, State Preparation and Dynamics of Ultracold Atoms in Higher Lattice Orbitals, *Phys. Rev. Lett.* **99**, 200405 (2007).

[26] Y. Tokura and N. Nagaosa, Orbital Physics in Transition-Metal Oxides, *Science* **288**, 462 (2000).

[27] G. Wirth, M. Ölschläger, and A. Hemmerich, Evidence for orbital superfluidity in the p-band of a bipartite optical square lattice, *Nat. Phys.* **7**, 147 (2011).

[28] H.-R. Xia, Z. Wang, Y. Wang, Z. Gao, and M. Xiao, Fully Flat Bands in a Photonic Dipolar Kagome Lattice, *Phys. Rev. Lett.* **135**, 176902 (2025).

[29] M. Milićević, T. Ozawa, G. Montambaux, I. Carusotto, E. Galopin, A. Lemaître, L. Le Gratiet, I. Sagnes, J. Bloch, and A. Amo, Orbital edge states in a photonic honeycomb lattice, *Phys. Rev. Lett.* **118**, 107403 (2017).

[30] C. Jörg, G. Queraltó, M. Kremer, G. Pelegrí, J. Schulz, A. Szameit, G. von Freymann, J. Mompart, and V. Ahufinger, Artificial gauge field switching using orbital angular momentum modes in optical waveguides, *Light: Sci. Appl.* **9**, 150 (2020).

[31] G. Cáceres-Aravena, D. Guzmán-Silva, I. Salinas, and R. A. Vicencio, Controlled Transport Based on Multiorbital Aharonov-Bohm Photonic Caging, *Phys. Rev. Lett.* **128**, 256602 (2022).

[32] R. A. Vicencio, Multi-orbital photonic lattices, *APL Photonics* **10**, 071101 (2025).

[33] J. Noh, J. Schulz, W. Benalcazar, and C. Jörg, Orbital frontiers: harnessing higher modes in photonic simulators, *Nanophotonics* **14**, 4273 (2025).

- [34] X. Li, E. Zhao, and W. Vincent Liu, Topological states in a ladder-like optical lattice containing ultracold atoms in higher orbital bands, *Nat. Commun.* **4**, 1523 (2013).
- [35] J. Schulz, J. Noh, W. A. Benalcazar, G. Bahl, and G. von Freymann, Photonic quadrupole topological insulator using orbital-induced synthetic flux, *Nat. Commun.* **13**, 6597 (2022).
- [36] M. Mazanov, D. Román-Cortés, G. Cáceres-Aravena, C. Cid, M. A. Gorlach, and R. A. Vicencio, Photonic Molecule Approach to Multiorbital Topology, *Nano Lett.* **24**, 4595 (2024).
- [37] S. Gross, N. Riesen, J. D. Love, and M. J. Withford, Three-dimensional ultra-broadband integrated tapered mode multiplexers, *Laser Photonics Rev.* **8**, L81 (2014).
- [38] T. A. Birks, I. Gris-Sánchez, S. Yerolatsitis, S. Leon-Saval, and R. R. Thomson, The photonic lantern, *Adv. Opt. Photonics* **7**, 107 (2015).
- [39] G. Rajeevan and S. Mukherjee, Nonlinear switch and spatial lattice solitons of photonic s–p orbitals, *Opt. Lett.* **50**, 297 (2025).
- [40] K. M. Davis, K. Miura, N. Sugimoto, and K. Hirao, Writing waveguides in glass with a femtosecond laser, *Opt. Lett.* **21**, 1729 (1996).
- [41] A. Szameit and S. Nolte, Discrete optics in femtosecond-laser-written photonic structures, *J. Phys. B: At. Mol. Opt. Phys.* **43**, 163001 (2010).
- [42] D. N. Christodoulides, F. Lederer, and Y. Silberberg, Discretizing light behaviour in linear and nonlinear waveguide lattices, *Nature* **424**, 817 (2003).
- [43] Y. Aharonov and D. Bohm, Significance of Electromagnetic Potentials in the Quantum Theory, *Phys. Rev.* **115**, 485 (1959).
- [44] T. Dubček, K. Lelas, D. Jukić, R. Pezer, M. Soljačić, and H. Buljan, The Harper-Hofstadter Hamiltonian and conical diffraction in photonic lattices with grating assisted tunneling, *New J. Phys.* **17**, 125002 (2015).
- [45] F. Nathan and M. S. Rudner, Topological singularities and the general classification of Floquet–Bloch systems, *New J. Phys.* **17**, 125014 (2015).
- [46] A. W. Snyder and J. D. Love, *Optical waveguide theory*, Vol. 175 (Chapman and hall London, 1983).
- [47] M. Zhang, C. Wang, Y. Hu, A. Shams-Ansari, T. Ren, S. Fan, and M. Lončar, Electronically programmable photonic molecule, *Nat. Photonics* **13**, 36 (2019).
- [48] K. Krupa, A. Tonello, B. M. Shalaby, M. Fabert, A. Barthélémy, G. Millot, S. Wabnitz, and V. Couderc, Spatial beam self-cleaning in multimode fibres, *Nat. photonics* **11**, 237 (2017).

- [49] F. O. Wu, A. U. Hassan, and D. N. Christodoulides, Thermodynamic theory of highly multimoded nonlinear optical systems, [Nat. Photonics **13**, 776 \(2019\)](#).
- [50] Y. Zhang, D. Bongiovanni, Z. Wang, X. Wang, S. Xia, Z. Hu, D. Song, D. Jukić, J. Xu, R. Morandotti, H. Buljan, and Z. Chen, Realization of photonic *p*-orbital higher-order topological insulators, [elight **3**, 5 \(2023\)](#).
- [51] S. Mukherjee and M. C. Rechtsman, Observation of unidirectional solitonlike edge states in nonlinear Floquet topological insulators, [Phys. Rev. X **11**, 041057 \(2021\)](#).

Supplementary Information

A. Fabrication of photonic *s-p* lattices

The photonic *s-p* lattices consist of optical waveguides with three-dimensionally modulated paths to implement the desired z -dependent couplings described in the main text, see Fig. 1. We employ femtosecond laser writing to fabricate the lattices inside a 120-mm-long borosilicate (BK7) glass material, Fig. S1(a). To this end, we use circularly polarized 260 fs (FWHM) laser pulses at 1030 nm central wavelength, 500 kHz repetition rate, and 380 nJ pulse energy. The laser beam was focused inside the glass material mounted on high-precision x - y - z translation stages (Aerotech). As mentioned in the main text, each single-mode waveguide (A site) in the lattice was inscribed by translating the glass material twice through the focal region of the laser beam at a speed of 4 mm/s. For the two-mode waveguides (B site), we increase the refractive index profile. The same two-scan method was employed to fabricate the B sites, with a vertical scan-to-scan separation of 5 μ m. To precisely tune the refractive index of the B site, we vary the translation speeds. The optimal translation speeds for the lower and upper scans were found to be 1 mm/s and 2 mm/s, respectively, to satisfy the phase-matching condition, $\beta_s^A = \beta_p^B$.

At the input ($z = 0$) of the lattice, the waveguides are well separated ($d_x = 40 \mu$ m and $d_y = 45 \mu$ m) such that the inter-waveguide couplings are negligible. Specifically, the neighboring waveguides are separated more along y (vertical) compared to the x direction, since the supported orbitals are elongated along the vertical direction. To switch on the $J_{1,3}^{sp}$ couplings, we first reduce the inter-site vertical spacing between the corresponding waveguides by synchronously bending them; see Figs. S1(b, c). Then the inter-site spacing is kept fixed for a certain propagation distance L and finally increased in a reverse manner to obtain a step-like variation of the couplings along z . As indicated in Fig. 1(b), due to the π phase difference between the lobes of the p orbital, the J_1^{sp} coupling is negative. The $J_{2,4}^{sp}$ couplings are varied in a similar manner; however, the waveguides are kept at 45-deg angle in the coupling region with the same orientation of the orbitals; see Fig. S1(d). This specific layout of the waveguides is important to implement positive-valued horizontal couplings.

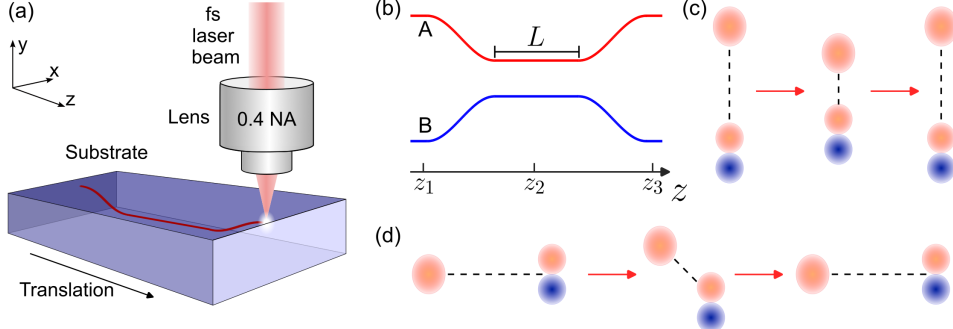


Figure S1. (a) Schematic of femtosecond laser writing. (b) Sketch showing the bending profiles of the A and B waveguides along the propagation direction. (c, d) Schematics of the cross-sections of relative positions of the *s* and *p* orbitals at three different *z* values (i.e., z_1 , z_2 , and z_3) for the J_3^{sp} and J_4^{sp} couplings, respectively.

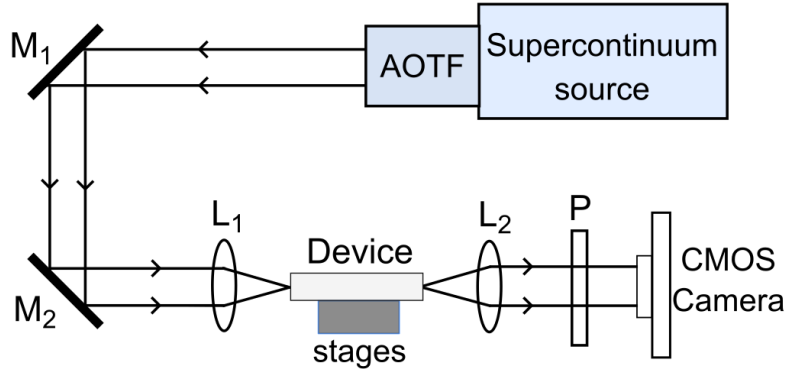


Figure S2. Schematic of the experimental characterization setup. A supercontinuum source, along with an acousto-optic tunable filter (AOTF), is used to generate wavelength-tunable collimated beam. Here, $M_{1,2}$ are silver-coated mirrors, $L_{1,2}$ are convex lenses, and P is a polarizer. For precise alignment, the photonic device is mounted on 4-axis stages with angular and translational control, and the two lenses are mounted on 3-axis translation stages.

B. Achieving the phase-matching condition

In the main text, we mentioned that the *s* orbital of A sites and the *p* orbital of B sites have the same propagation constants, i.e., $\beta_s^A = \beta_p^B$. Here, we provide experimental evidence to support this claim. The inset at the top of Fig. 1(a) shows the schematic of the refractive index profiles (scaled by the free-space wavevector k_0) of A and B sites. It is possible to control the waveguide refractive index contrast by either tuning the average

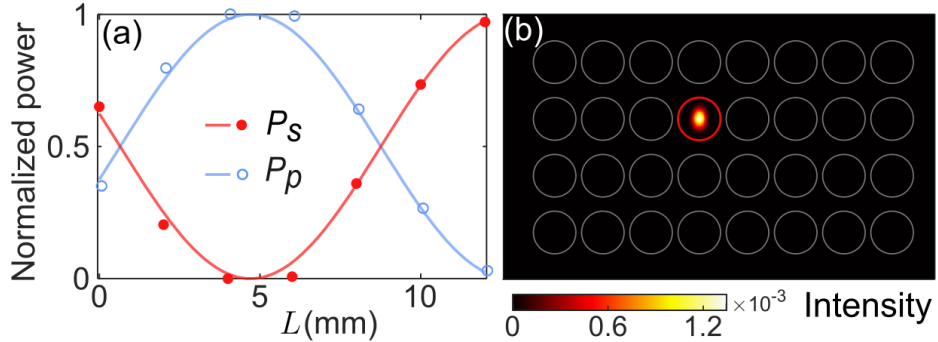


Figure S3. (a) Normalized output power in the s and p orbitals (P_s and P_p) as a function of propagation distance L . The solid lines are obtained numerically. The complete transfer of light from the s to the neighboring p orbital (near $L=4.75$ mm) confirms the phase-matching condition, $\beta_s^A = \beta_p^B$. (b) Experimentally measured output intensity distribution in the s - p lattice when light is launched at the s orbital of the B site (red circle). The absence of tunneling into the lattice confirms that the propagation constant detuning of this mode dominates over the couplings, i.e., $(\beta_s^B - \beta_p^B)/J_{sp} \gg 1$.

laser power or the translation speeds of fabrication. For our purposes, we optimize the translation speeds while keeping the fabrication power fixed. To estimate the difference of β_s^A and β_p^B , we fabricated seven sets of bendy s - p couplers with a variable interaction length L . These devices were characterized using horizontally-polarized low-power light at 980 nm wavelength, generated by a supercontinuum source; see Fig. S2. The near-Gaussian beam emitting from the source is focused to the s orbital at the input, and the output powers at the s and p orbitals (P_s and P_p) are measured as a function of L . As shown in Fig. S3(a), the optical power from the s orbital completely transfers to the p orbital of the neighboring site, confirming the phase-matching condition $\beta_s^A = \beta_p^B$. The phase-matching condition in our devices were found to be wavelength dependent for a given set of fabrication parameters.

As mentioned before, the s orbital of B site is largely detuned, i.e., $\beta_s^B - \beta_s^A \gg J_{sp}$. To validate this experimentally, we launch light at the s orbital of the B site and observe that the light does not spread in the lattice; see Fig. S3(b). This observation also implies that the tunneling of light from the s orbital of the A site to the s orbital of the B site would be negligible. In other words, the dynamics of optical fields in our photonic lattices can be effectively described by the discrete Schrödinger-like equation Eq. (1) containing the s - p orbital couplings.

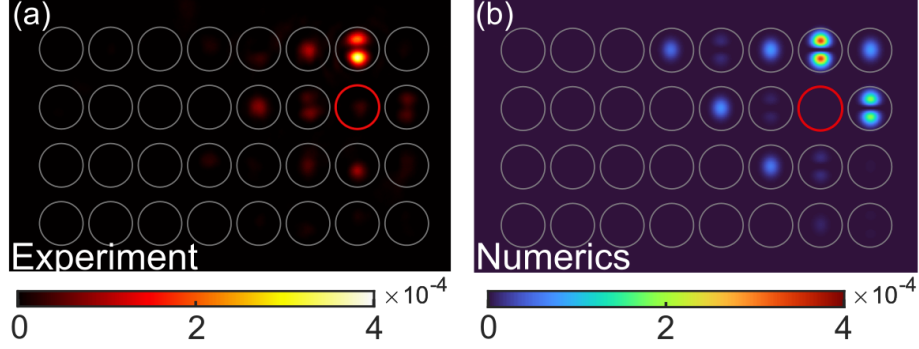


Figure S4. (a) Experimentally measured output intensity distribution in the *s-p* lattice when light is coupled into the *s* orbital of the A site (red circle). (b) Numerically obtained intensity pattern corresponding to (a).

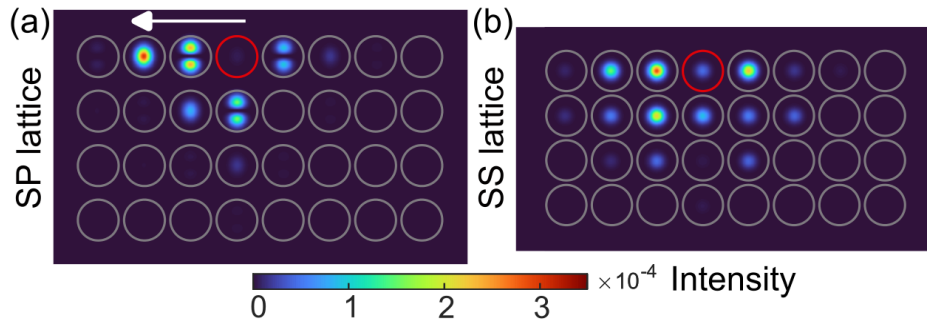


Figure S5. Numerically computed output intensity distributions in the lattice associated with Fig. 4, providing an estimated value of $\Lambda = 0.3\pi/2$.

C. Estimation of Λ

As highlighted in Fig. 3, the topology of our *s-p* orbital photonic lattices is captured by the parameter $\Lambda_m = |\int J_m^{sp}(z) dz|$, where the integral is carried over the m -th quarter of the driving period. We estimate the Λ -values by comparing the experimental and numerical output intensity distributions in the lattices. For example, Fig. S4(a) presents the intensity distributions for input excitation at a bulk site. The associated numerical result obtained by R-squared maximization is shown in Fig. S4(b). By considering four such data sets with different initial excitations, the mean and standard deviation of Λ were found to be $0.76\pi/2$ and $0.02\pi/2$, respectively. The numerical results associated with the second set of *s-p* and *s-s* lattices in Figs. 4(a, b) are presented in Fig. S5. In this case, the Λ -values were found to be $0.3\pi/2$ with a standard deviation of $0.04\pi/2$.